Supplemental Material

Spectroscopy along Flerovium Decay Chains: Details on Experiment, Analysis, ^{282}Cn, and Spontaneous Fission Branches

A. Såmark-Roth,[1*] D.M. Cox,[1] D. Rudolph,[1] L.G. Sarmiento,[1] M. Albertsson,[1] B.G. Carlsson,[1] J.L. Egido,[2] P. Golubev,[1] J. Heery,[3†] A. Yakushev,[4,5] S. Åberg,[1] H.M. Albers,[4] M. Block,[4,5,6] H. Brand,[4] T. Calverley,[3] R. Cantemir,[4] R.M. Clark,[7] Ch.E. Düllmann,[4,5,6] J. Eberth,[8] C. Fahlander,[1] U. Forsberg,[1] J.M. Gates,[7] F. Giacoppo,[4,5] M. Götz,[4,5,6] S. Götz,[4,5,6] R.-D. Herzberg,[3] Y. Hrabar,[1] E. Jäger,[4] D. Judson,[3] J. Khuyagbaatar,[4,5] B. Kindler,[4] I. Kojouharov,[4] J.V. Kratz,[6] J. Krier,[4] N. Kurz,[4] L. Lens,[4,6‡] J. Ljungberg,[1] B. Lommel,[4] J. Louko,[9] C.-C. Meyer,[5,6] A. Mistry,[10,4] C. Mokry,[5,6] P. Papadakis,[3§] E. Parr,[4] J.L. Pore,[7] I. Ragnarsson,[1] J. Runke,[4,6] M. Schädel,[4] H. Schaffner,[4] B. Schausten,[4] D.A. Shaughnessy,[11] P. Thörle-Pospiech,[5,6] N. Trautmann,[6] J. Uusitalo,[9]

[1] *Department of Physics, Lund University, 22100 Lund, Sweden*
[2] *Departamento de Física Teórica and CIAFF, Universidad Autónoma de Madrid, 28049 Madrid, Spain*
[3] *Department of Physics, University of Liverpool, Liverpool L69 7ZE, United Kingdom*
[4] *GSI Helmholtzzentrum für Schwerionenforschung GmbH, 64291 Darmstadt, Germany*
[5] *Helmholtz Institute Mainz, 55099 Mainz, Germany*
[6] *Department Chemie-Standort TRIGA, Johannes Gutenberg-Universität Mainz, 55099 Mainz, Germany*
[7] *Nuclear Science Division, Lawrence Berkeley National Laboratory, Berkeley, CA 94720, USA*
[8] *Institut für Kernphysik, Universität zu Köln, 50937 Köln, Germany*
[9] *Department of Physics, University of Jyväskylä, 40014 Jyväskylä, Finland*
[10] *Institut für Kernphysik, Technische Universität Darmstadt, 64289 Darmstadt, Germany and*
[11] *Nuclear and Chemical Sciences Division, Lawrence Livermore National Laboratory, Livermore, California 94550, USA*

(Dated: January 7, 2023)

This Supplemental Material provides further details of data analysis aspects concerning the nuclear structure studies of α-decay chains stemming from isotopes of element 114, flerovium.

I. DETAILS OF THE DATA ANALYSIS

In Sec. I A the method that was used to derive N_{random}, i.e., the number of apparent decay chains of a given type expected to arise randomly from background is presented. A likelihood assessment of missing events, and in particular missed implantation events, is outlined in Sec. I B. Section I C focuses on the treatment of so-called escape events, i.e., when α-decay events leave merely a fraction of their decay energy only in the central double-sided silicon strip detector (implantation DSSD). The procedure used to derive α-decay energies from measured energies in the implantation DSSD is described in Sec. I D. Finally, comments on germanium detector data processing and randomly correlated photon coincidences are subject of Sec. I E. Table I lists information on three decay chains which were considered as candidates originating from ^{289}Fl. The format is the same as in Tables I in the Supplemental Materials of Refs. [1, 2], respectively.

A. Random chains

The number of chains of a given type expected to arise from random background across the whole implantation detector, N_{random}, was calculated for all candidate flerovium decay chains based on the method outlined in Refs. [3, 4]. The probability for one or more events of a certain type X to occur was calculated assuming Poisson distributions:

$$P(X \geq 1) = 1 - P(X = 0) = 1 - e^{-\lambda}, \qquad (1)$$

where λ represents the expected number of events X. For the flerovium decay chains in the current analysis, an event type was defined by the measured rate, R, of this event during the experiment and the time window, Δt, within which it was accepted. The expected number of events for decay step i in pixel p corresponds to:

$$\lambda_i^p = R_i^p \times \Delta t_i, \qquad (2)$$

where R_i^p is the pixel rate of the event in decay step i, derived from experimental spectra such as that in Fig. 2(b). The used time window, Δt_i, is the time interval in which the event is accepted for decay step i. Pixel rates were

*anton.samarkroth@gmail.com
†Present address: Department of Physics, University of Surrey, Guildford GU2 7XH, United Kingdom.
‡Present address: Institut für Physikalische Chemie und Radiochemie, Hochschule Mannheim, 68163 Mannheim, Germany.
§Present address: STFC Daresbury Laboratory, Daresbury, Warrington WA4 4AD, United Kingdom.

TABLE I: Information on observed correlated α-decay chains possibly stemming from the odd-A flerovium isotope ^{289}Fl. Mid-target beam energies in the laboratory frame, $\langle E_{\rm lab}\rangle$, and the center-of-mass frame, $\langle E_{\rm com}\rangle$, as well as target isotope are provided. Energies of the implanted recoils, $E_{\rm rec}$, the implantation detector strip numbers in x and y, and the assigned isotope of chain origin are listed for each chain. For each decay step, i, the decay energy, E_i, correlation time, Δt_i, and, if in prompt coincidence, photon energies, $E_{\rm ph}$ are given. For a spontaneous fission (SF) event, the number of prompt hits in the Ge-detector crystals, $N_{\rm Ge}$, is provided instead of any specific photon energy. $N_{\rm random}$ indicates the number of chains of a given type expected to arise from random background. Entries in bold were recorded during beam-off periods. Entries in italic relate to tentative or insecure assignments, typically in connection with a missing event in a chain. Uncertainties of individual energy measurements are ≤ 10 keV at typical α-decay energies of 9-10 MeV in the implantation detector. This uncertainty is worse, ≈ 20 keV, for reconstructed events because of the energy straggling in the deadlayers of the Si detectors.

No.	$\langle E_{\rm lab}\rangle$ (MeV) $\langle E_{\rm com}\rangle$ (MeV) target[a]	$E_{\rm rec}$ (MeV) pixel (x,y) isotope	E_1 (MeV) Δt_1 (s) E_{ph} (keV)	E_2 (MeV) Δt_2 (s) E_{ph} (keV)	E_3 (MeV) Δt_3 (s) E_{ph} (keV)	E_{SF} (MeV) Δt_{SF} (s) $N_{\rm Ge}$	$N_{\rm random}$
30	237	missing[b]	**9.55(2)**[c]	**0.47(1)**[d]		**199**[e]	7×10^{-3}
	36.5	(19,18/17)	-	**6.956**		**11.833**	
	^{244}Pu	—[f]	-	-		**7**	
31	237	missing[b]	**9.62(2)**[c]	**0.35(1)**[d]		**230**[g]	7×10^{-3}
	36.5	(21/22,12)	-	**27.451**		**101.139**	
	^{244}Pu	—[f]	**106(1)**	[h]		**4**	
32	237	17.7[i]	missing	9.11(1)		**219+1**	0.7
	36.5	(30,16)	-	*38.487*		**7.449**	
	^{244}Pu	—[f]	-	-		**1**	

[a]For the first part of the experiment, the target wheel comprised one segment of enriched ^{242}Pu and three segments of enriched ^{244}Pu. For the second part of the experiment, all four segments of the target wheel were made of enriched ^{244}Pu. See Sec. II main article for details.
[b]Another 14.5-MeV implant candidate event 0.580 s earlier.
[c]Reconstructed event (cf. Sec. I C). Detected energies in the implantation detector and in the box DSSSD were: chain 30: 0.92(1) and 7.12(1) MeV; chain 31: 0.59(1) and 8.42(1) MeV.
[d]Escape event. See Sec. I C for details.
[e]Non-fusion product implant candidates 11 and 27 s prior to the fission event concluding the decay chain.
[f]This chain has been disregarded. See Sec. I A.
[g]Non-fusion product implant candidates 4 and 29 s before fission event concluding the decay chain.
[h]Delayed γ ray(s) observed within $\Delta t = [1, 7]$ µs.
[i]Another 12.6-MeV implant candidate event 75.052 s earlier.

determined for full-energy (including reconstructed) α-decay events, escape-α events, $\alpha_{\rm esc}$, and spontaneous-fission events, separately for ^{286,288}Fl and ^{289}Fl chain members as well as for each decay step, as presented in Table II. The total number of random chains within a pixel is given by the product of the probabilities for each decay step, i, to occur, and the total number of recoil events throughout the entire experiment in pixel p, denoted $N^p_{\rm recoil}$. The presented total number of random chains in, e.g., Table I, $N_{\rm random}$, for a Fl-decay chain with $N_{\rm steps}$ decay steps, is the sum of the possible events for all 1024 pixels of the implantation detector:

$$N_{\rm random} = \sum_{p=1}^{1024} N^p_{\rm recoil} \prod_{i=1}^{N_{\rm steps}} (1 - e^{-\Delta t_i \times R^p_i}) \qquad (3)$$

In the case of a missing recoil event for a decay chain, $N_{\rm recoil}$ was replaced by the total number of events defined by the first decay step and the product was initiated for $i = 2$. If the α-decay for step i was missing, it was skipped and Δt_{i+1} was replaced by $\Delta t_i + \Delta t_{i+1}$.

Based on the above-described method, the candidate chain 32 was disregarded because the expected number of random chains was too large, $N_{random} = 0.7$, for its type of chain. Also candidate chains 30 and 31 were disregarded in further analysis and interpretation steps, despite their expected number of random chains being only $N_{random} = 7\times10^{-3}$. There are several reasons for that: (*i*) Their implantation signals were missing. (*ii*) Their first α-decay steps were reconstructed to rather low energies in an energy region where we found an excess of reconstructed events compared with full-energy events [cf. Fig. 2(d)]. An intricate explanation of that excess of reconstructed events at $E_{\rm det} \approx [9.5, 9.8]$ MeV was linked to very fast two-α decay sequences across, e.g., neutron number $N = 128$; one of the two energetic α particles hits a box DSSD and the second α particle escapes full detection. In this case, the sum of two hits in the implantation DSSD is reconstructed with the hit in the box DSSD rendering an invalid reconstructed energy. (*iii*) Low-energy escape-α events marked the sec-

TABLE II: Criteria used in the correlation search and in the calculation of the expected number of random chains for defined event types for each α-decay step of chains starting with ^{289}Fl and ^{286,288}Fl. Total rates of the different event types across the implantation detector, i.e., $\sum_{p=1}^{1024} R_i^p$, are given in the last column. The table starts with generic types, i.e., independent of decay step, namely recoil events, escape-α events ($\alpha_{\rm esc}$), and spontaneous-fission events (SF). For $\alpha_{\rm esc}$-decay steps, the time window is the same as defined for the corresponding α-decay step. See text for details.

Isotope	Decay step	Type	Beam status	Energy window (MeV)	Δt (s)	Total rate (s^{-1})
		recoil[a]	ON	[11.0,20.0]		1.4
		$\alpha_{\rm esc}$	ON	[0.3,1.5]		30.1
			OFF			10.2
		SF	ON	[150,250]		3×10^{-3}
			OFF	[100,300]		4×10^{-5}
^{289}Fl	1	α	ON	[9.5,10.3]	10	0.3
			OFF	[9.5,10.5]	20	7×10^{-4}
	2	α	ON	[9.0,9.7]	150	0.3
			OFF	[8.8,9.7]	300	1×10^{-2}
	3	α[b]	ON	[8.5,9.5]	50	0.5
			OFF		110	0.01
	4	SF	ON/OFF		1	
^{286,288}Fl	1	α	ON	[9.4,10.5]	7	0.4
			OFF		7	9×10^{-4}
	2	α[b]	ON	[9.0,10.0]	1	0.4
			OFF		1	3×10^{-3}
	3	SF	ON/OFF		1	

[a]Event had to be anti-coincident with signal in veto DSSD to be considered a recoil.
[b]If the decay chain was found to terminate with spontaneous fission in this decay step, the beam-off Δt was used.

ond α-decay step, cf. Sec. I C. (*iv*) There were at least two implantation events of transfer reaction products between the escape-α events and the concluding SF event, respectively. (*v*) In case of chain 30, the energy measurement of the fission event was split between neighboring strips of the implantation detector, but not the signals of the preceding *escape*-like energies in the implantation detector.

A final remark is to be made on the random rates compared between beam-on and beam-off periods and its effect on our ability to deduce whether a decay chain stems from random correlations. The most challenging case is a decay chain starting with an implantation event, followed by only one α-decay member within [8.5,10.5] MeV, and then terminating by spontaneous fission. Before expecting one random chain in the current experiment, it would be possible to open a time window of merely 15 s for α decays taking place during periods with beam on. Correspondingly, one could allow a time window of a striking 800 s for α decays happening during beam-off periods.

B. Missing recoils and decay events

In the present data set (cf. Tables I in the Supplemental Materials of Refs. [1, 2]), four out of 29 decay chains assigned to originate from flerovium isotopes were missing an implantation event. This corresponds to $\approx 14\,\%$. Figure 1(a) shows the rate of trigger requests and accepted triggers by the data acquisition system as a function of time after the start of the beam pulse (5 ms beam on, 15 ms beam off). For these measurements, the average beam intensity was 3.3 pμA on the Pu target during beam on. It can be seen that the rate of trigger requests (blue curve) was significantly higher than the rate of the accepted triggers (red curve) during the beam pulse, corresponding to the time interval [0,5] ms. After the beam pulse, corresponding to the time interval [5,20] ms, the two rates were nearly identical. In case the beam shut-off routine was activated, the difference of the two rates is negligible, i.e., practically no events could be missed.

Quantitatively, $\approx 21\%$ of the trigger requests were not accepted during the beam pulse. The measured rates in Fig. 1(a) were used to derive an average deadtime of ≈ 190 μs. This value is well in line with the time difference between subsequently recorded events, which is displayed in Fig. 1(b). However, there are two types of requested triggers, namely: (i) trigger requests occurring outside of a trigger window, due to readout deadtime, and (ii) trigger requests occurring inside of a trigger window, although another trigger request caused the accepted trigger. Signals generating trigger requests of

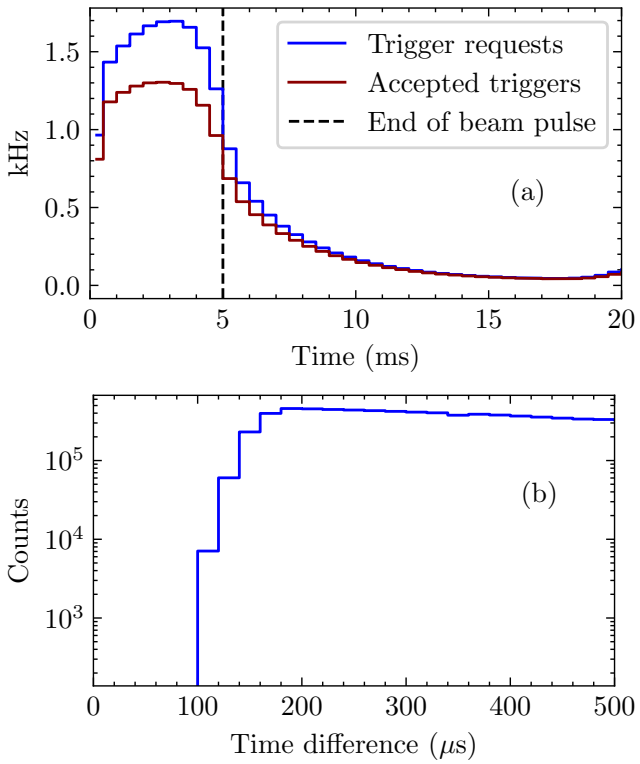

FIG. 1: (Color online) (a) Rate of trigger requests and accepted trigger as a function of time after the start of the beam pulse. The end of the beam pulse is denoted by the dashed line at 5 ms, the repetition rate is 20 ms. (b) Time difference between subsequent recorded events.

type (i) are missed, while those of type (ii) are not, because they are contained in the recorded traces. In the experiment, 80-μs long traces were recorded for the silicon detector channels with a 10 μs delay for the rising edge of the triggering pulse. For 70 μs following the event trigger they could be properly processed by the pulse-shape analysis routine, i.e., the effective deadtime is only $(190-70)$ μs =120 μs. Consequently, one expects to miss $\approx 21\,\% \times 120/190 \approx 14\,\%$ of the events during beam-on periods. This estimate is in good agreement with the above-mentioned value of 14 % missed recoil-implantation events.

During the full 20-ms beam cycle, the probability to miss any event of interest because of data acquisition system deadtime was determined to $\approx 8\,\%$ based on Fig. 1(a) and the 120/190-correction factor described earlier. For beam-off periods, the value descreases to $\approx 6\,\%$. In the experiment, three out of 47, i.e., $\approx 6\%$ of the α-decay steps were missing, namely in chains 15, 24, and 29. However, a somewhat lower number is expected due to a possible over-assignment of escaping α events together with the fact that when the 200-s or 300-s long beam shut-off routine was activated, which was the case for 16 out of the 29 assigned chains, one does not expect to miss any decay event a few ms after activation.

C. Escape-alpha event candidates

For about 80 % of the α decays from nuclei in the implantation detector, their energy can be determined. This is because the α particle either deposits its *full* energy in the implantation detector itself ($\approx 50\,\%$), or it deposits part of its energy in the implantation detector and the remaining part of its energy in one of the box DSSDs positioned upstream ($\approx 30\,\%$) [5]. For the latter, the full α energy is *reconstructed* by correcting for energy losses in deadlayers, present both when leaving the implantation-DSSD pixel and when entering a box-DSSD pixel. Deadlayer thicknesses were experimentally determined pixel by pixel prior to the experiment according to procedures outlined in, e.g., Ref. [6]. In the remaining $\approx 20\,\%$ of the cases, however, the emitted α particle deposits only part of its energy in the implantation DSSD, while not entering any of the four upstream box DSSDs. These α particles are *escaping* complete detection.

For the present experiment, a trigger threshold energy down to ≈ 120 keV in the implantation detector implied a significant number of low-energy signals to be handled and assessed during the rather long correlation times of anticipated flerovium decay chains, even during beam-off periods. Therefore, at an early stage of the analysis, a valid escape-α candidate event, denoted $\alpha_{\rm esc}$, had to fulfill the following three criteria:

1. Event during beam-off period.
2. More than 300 keV energy deposited in the implantation DSSD.
3. Anti-coincidence with signals in any of the box and in particular the veto DSSDs.

In general, the lower limit on the deposited energy, 300 keV, was guided by GEANT4 simulations [7, 8], which resulted in the spectrum shown in Fig. 2(a). In the simulation, α particles with $E_\alpha = 9.14$ and 9.92 MeV were emitted isotropically from a depth of 5.0(6) μm [9] in the implantation detector. The spectrum was incremented with events for which solely the implantation detector registered a hit. From such a simulation, a relative likelihood to observe escaping α particles within certain energy ranges can be determined. The energy windows and the corresponding likelihoods are provided in the first row of Table III and are shown as dashed vertical lines in Fig. 2(a). The division into three energy regions is motivated by the simulated and measured spectra in Figs. 2(a) and (b). The low-energy 'peak' of the spectrum in Fig. 2(a) relates to α particles emitted upstream, i.e., into space where no box detectors can be hit. The remaining part, $E > 1.5$ MeV, is then split at 5.0-MeV in energy. Beyond that energy, background activity from transfer reaction channels, which kept building up during the experiment, was dominating the rate, especially in the respective α peaks visible in Fig. 2(b). Furthermore, based on the simulated spectrum in Fig. 2(a), the likelihood that the emitted 9.14 and 9.92 MeV α-particles deposit their energy within $[E_\alpha - 0.9, E_\alpha - 0.1]$ MeV is

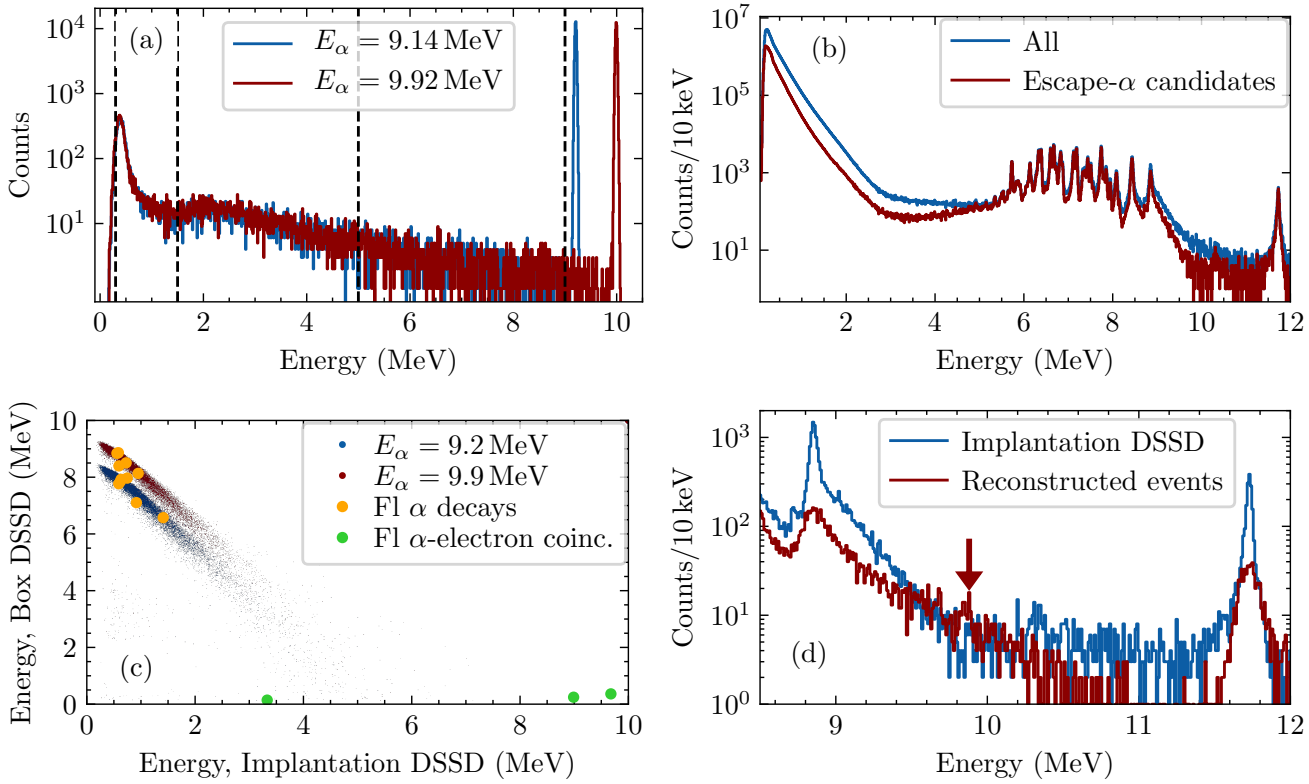

FIG. 2: (Color online) (a) Energy spectra of GEANT4-simulated α particles emitted isotropically from a depth of 5.0(6) μm in the implantation detector with E_α = 9.14 and 9.92 MeV. Events were considered when energy was solely deposited in the implantation detector. Vertical dashed lines represent limits for the energy ranges considered in Table III. (b) Beam-off energy spectrum measured with the implantation detector during the complete experiment (blue). The spectrum in red fulfills all three escape-α criteria defined in the text. (c) Simulated two-dimensional correlation spectrum of coincident events in the implantation detector and any of the box DSSDs for α particles emitted isotropically from a depth of 5.0(6) μm in the implantation detector with E_α = 9.14 and 9.92 MeV, respectively. The eleven observed reconstructed events (cf. Tables I in Supplemental Materials in Refs. [1, 2]) are marked by filled orange circles. The three α-electron coincidences are marked with filled green circles. (d) The spectrum in blue corresponds to events measured beam-off and with only the implantation detector. The spectrum in red shows reconstructed events focusing on the energy region of main interest, $E = [8.5, 12.0]$ MeV. The arrow indicates a region where the number of counts in the reconstructed spectrum exceeds that of the implantation DSSD.

smaller than 2×10^{-3}. Hence it is unlikely that α-decays with energies in the [8.5,10.5] MeV range detected solely in the implantation DSSD, actually stem from escape-α events.

A considerable number of β decays (of transfer reaction products) were seen, which manifest in events for which low-energy signals in the implantation detector were observed in prompt coincidence with low-energy signals in the box and/or veto DSSDs. This becomes visible in the difference between the blue and red spectra in Fig. 2(b).

TABLE III: Relative likelihood of observing escaping α particles derived from the GEANT4 simulated spectrum displayed in Fig. 2(a). The observed rate of escape-α candidate events across the whole implantation detector within these three energy ranges is provided, based on the measured spectra shown in Fig. 2(b). See text for details.

Energy window (MeV)	[0.3, 1.5)	[1.5, 5.0)	[5.0, 9.0]
Relative likelihood α_{esc}	0.64	0.28	0.08
Rate α_{esc} (s^{-1})	12.7	0.09	0.17

The energy spectrum of the implantation detector during beam-off periods for the full experiment, along with the corresponding spectrum for escape-α candidate events according to the criteria listed above, is presented in Fig. 2(b). Rates of α_{esc} within certain energy windows were determined from the spectrum in red. The resulting values are given in the second row of Table III. It is worth noting that applying the escape-α criteria suppresses the rate within [0.3,1.5] MeV in the energy spectrum by $\sim$ 70%. The veto DSSD anti-coincidence criterion stands for $\sim$ 70% of this suppression. The excess of counts in the blue spectrum in Fig. 2(b) in the energy range 9 to 10 MeV relates to a relatively large number of reconstructed α events and to known, fast α-β correlations discussed in more detail in Sec. III in the main

article.

Based on the same simulation, expected coincidence events between hits in the implantation detector and any of the box DSSDs are shown in Fig. 2(c). For the experiment, such events are subject to reconstruction, taking into account the angle-dependent effective thicknesses of the deadlayers, known pixel-by-pixel for all detectors. The 11 reconstructed events listed in Tables I in Supplemental Materials in Refs. [1, 2] are overlaid as filled orange circles. They are very well in line with the simulations. The three coincidences in the implantation detector and $E < 0.4$ MeV in the box detectors provided in Tables I in Supplemental Materials in Refs. [1, 2] are indicated by filled green circles in Fig. 2(c). The events with $E > 8$ MeV, i.e., those with presumed full α-energy deposited in the implantation DSSD, are *incompatible* with plain α-particle emission, which would in that case be subject to reconstruction. On the other hand, the event in chain 26, where 3.33(1) MeV is deposited in the implantation DSSD and 0.14(1) MeV in a box DSSD, may be compatible with a reconstructed event. However, based on the simulated spectrum in Fig. 2(c), the likelihood that [1.5,5.0] MeV is deposited in the implantation DSSD and [50,1000] keV in a box DSSD is $\approx 10^{-3}$. Therefore, the three coincidence events find their most likely explanation in α-electron coincidences (cf. Sec. III main article).

Figure 2(d) shows beam-off full-energy implantation DSSD-only (blue) and reconstructed (red) spectra in the energy region of interest for α particles in connection with decay chains originating from flerovium isotopes. Besides the expected worsened energy resolution, the reconstructed events provide an energy spectrum very similar to the full-energy events, not the least because of the precise knowledge of deadlayer thicknesses as a function of emission angle. Note, however, the relative excess of counts at reconstructed energies between 9.5 and 9.8 MeV (see also Sec. I A).

In the following, we detail the reasoning around each of the six candidate escape events observed as part of the 29 decay chains associated with flerovium isotopes. Two of these were disregarded.

1. Disregarded escape candidate in chain 19

A 5.65(1)-MeV event was registered 18.0 s prior to the fission event. The probability to observe at least one [5,9] MeV event within the time between the preceding α decay and the fission, $\Delta t = 53.2$ s, is close to 0.01, see Eq. (1). Because the decay energy is close to an α-peak energy of a transfer reaction channel (^{224}Ra), and because this chain was observed towards the end of the experiment, we classified this event as random background, though correlating it with decay chain 19 had a similar likelihood. To support the removal of this escape candidate, we conducted a separate search for correlated α-decay events of the daughter and granddaughter of ^{224}Ra in that pixel: indeed, 138 s after the 5.65(1) MeV event followed another α-decay event with 6.80(1) MeV, which is in good agreement with the known decay characteristics of ^{216}Po [10], the granddaughter of ^{224}Ra.

2. Valid escape event in chain 3

The time between the implantation event and the fission event is very short, $\Delta t < 0.13$ s. The random probability to observe at least one event in the energy range [5,9] MeV within this brief period is $\approx 10^{-5}$, while the relative likelihood for a flerovium α-decay escape energy to be within the energy range [5,9] MeV is 0.08 (see Table III). Corrected for the energy of a recoil with mass $A = 224$, the observed event with $E_\alpha = 5.68(1)$ MeV may correspond to a peak at 5.73 MeV in Fig. 2(b), which in turn might relate to ^{224}Ra (see above). In that case, its progenies might be be found at later times, past the registered fission. To this end, a dedicated search for up to 500 s after the fission event was performed, but no indications of decays resembling that of the daughter or granddaughter of ^{224}Ra in the pixel of interest could be found. Note that there is no indication of charge division for the recoil implantation event and the spontaneous fission event for this chain. Therefore, this event was included as an escape in chain 3.

3. Valid escape event in chain 26

A 3.33(1)-MeV escape event was observed within the time interval, $\Delta t = 92.6$ s, between the first α decay, which activated the 300-s beam shut-off, and the concluding fission event of chain 26. The probability to observe at least one event in the energy interval [1.5,5.0] MeV within that period is $\approx 8 \times 10^{-3}$. The relative likelihood for a flerovium α-decay escape energy to be within [1.5,5.0] MeV is, however, 0.28. Based on the above arguments, this event was included as an escape in chain 26.

4. Low-energy escape candidates in chains 22 (valid), 27 (disregarded), and 28 (valid)

A total of three low-energy, $E = [0.3, 1.5]$ MeV, escape candidates were observed. The random probabilities to observe at least one such event within the respective time intervals, namely 57.6 s for chain 22, 46.0 s for chain 27, and 278.6 s for chain 28, are ≈ 0.5, ≈ 0.4, and ≈ 1.0, respectively. Note, however, that all three escape candidate events occurred during periods for which the beam shut-off was activated by the preceding α-decay event. This implies a considerably reduced overall event rate. For instance, for chain 28, four random escape events were expected within 278.6 s [see also Eq. (2)], but only one was observed. Since the relative likelihood for a flerovium α-decay escape energy to be within

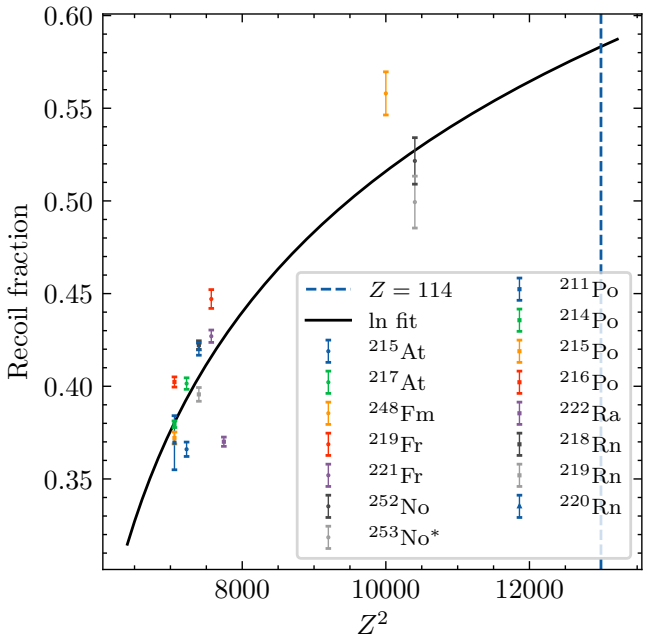

FIG. 3: (Color online) Calculated values of the recoil fraction, r, for a collection of well-known α-decaying nuclei. For ^{253}No, the star indicates the selection of α-decay events in prompt coincidence with the 280-keV, $9/2^- \rightarrow 7/2^+$ ground-state γ-ray transition in ^{249}Fm. A logarithmic least-squares fit was used to extrapolate toward $r \approx 0.58$ applied in the flerovium region ($Z = 114$).

[0.3,1.5] MeV is 0.64, i.e., of the same order of magnitude, the (non)assignment of the escape events in chains 22, 27, and 28 required guidance by previously reported and presently observed decay chains associated with ^{289}Fl. The events in chain 22 and chain 28 were included in their respective chain while the escape candidate in chain 27 was disregarded.

D. Recoil fraction and alpha-decay energies

For nuclei decaying in the implantation detector of TASISpec, the measured decay energy of an α event includes both the energy deposited along the track of the α particle, E_α, and along the track of the recoiling nucleus, $E_{\rm rec}$. Because of differences in charge-production and charge-collection for the two cases, effectively only a fraction, r, of $E_{\rm rec}$ is recorded [11]. The detected energy, $E_{\rm det}$, becomes:

$$E_{\rm det} = E_\alpha \cdot \left(1 + \frac{4}{(A-4)} \cdot r\right) \qquad (4)$$

The recoil fraction, r, was determined by the investigation of well-known α emitters produced during calibration runs prior to the main experiment, namely ^{252,253}No and ^{248}Fm via the reaction ^{48}Ca+^{206,207}Pb [12], as well as mass $A \approx 220$ transfer reaction products throughout the main experiment. By comparing calculated recoil fractions with Eq. 4 and known α-decay energies [10], a dependence on Z^2 of the decaying nucleus was concluded. Using a logarithmic least-squares fit to the data, which is shown in Fig. 3, a general description of the recoil fraction was determined. The resulting E_α values lie within $\pm$10 keV of the tabulated data and cover the interval E_α=[6,12] MeV. For the flerovium and copernicium isotopes of interest, $r \approx 0.58$ can be read from Fig. 3.

In a previous experiment on flerovium decay chains behind TASCA [13, 14], $r = 0.40$ was used to determine the α-particle energies. For consistency, α-particle energies listed in Table IV of Ref. [14] were recalculated with the respective r values from Fig. 3 prior to combining former and present data sets. The average correction factor was ≈ 0.9975, implying a reduction of ≈ 25 keV of the former α-particle energies.

The full width at half maximum (FWHM) for α-decay lines in the range $E_\alpha = [6, 12]$ MeV increases from 31 to 42 keV. The FWHM for reconstructed events is approximately constant at some 150 keV across the whole range. For instance, the single ^{212}Po 11.7-MeV line, which is part of the spectra shown in Fig. 2(d), reveals values of FWHM = 42 and 155 keV, for events detected solely in the implantation DSSD and for reconstructed events, respectively.

E. Germanium detector data

All germanium crystals - seven in the Cluster detector and the $4 \times 4 = 16$ of the Compex detectors - were operated in coincidence with charged-particle decays triggering the data acquisition. Their signals were processed by commercial Struck SIS3302 100-MHz, 16-bit sampling ADCs. The parameters of their built-in pulse-shape analysis firmware routine were optimized for low-energy photons prior to the experiment. The processing of the recorded flat-top energy, signal baseline, and time followed procedures described in Refs. [15, 16]. A similar condition for *prompt* coincidences with a photon-energy dependent 300-400 ns time window with respect to the particle trigger, was implemented. In a period $\Delta t = [1, 7]$ μs after the prompt time window, hits in the germanium detectors were labeled as *delayed coincidence*.

The germanium detectors were calibrated with two-split linear functions based on ^{133}Ba and ^{152}Eu source measurements prior, during, and after the experiment. In-beam energy re-calibrations were achieved by monitoring the spectral positions of 139.7-keV and 1779.0-keV lines from (n,γ) reactions on ^{74}Ge and ^{28}Al, respectively, in conjunction with the 511.0-keV e^+e^- annihilation peak. The respective spectra used data taken during beam-off periods. In this way, potential drifts in amplification of all detector channels throughout the full experiment were accounted for. An uncertainty of $\pm$1 keV of photon energies resulted from an upper limit of deviations of measured photon peak positions from tabulated

photon energies across the energy range of interest. One germanium crystal was noisy compared to the others, and an uncertainty of ±2 keV was assigned to it.

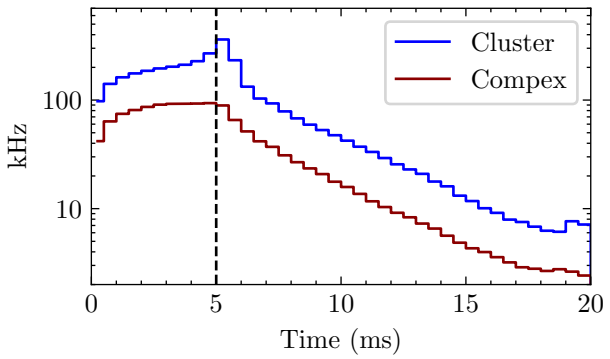

FIG. 4: Ge-trigger rates as a function of the start of each beam pulse for single crystals in the Cluster and Compex detectors. The end of beam pulse is denoted by the dashed vertical line. For these measurements, the average pulse beam intensity was 3.1 μA (particle) on the Pu target.

Dedicated measurements to understand background and random correlations of photons were taken with Ge-detectors triggering the readout for a brief period [12]. At that time, 90% of the 5-ms beam pulses reached the experimental cave, at an average pulse intensity of 3.1 pμA on the Pu target. Figure 4 shows rates of trigger requests from two germanium crystals as a function of time after the start of the beam pulse. Thanks to the pulsed beam structure of the GSI UNILAC beam, the background rates in both the germanium detectors as well as the silicon detectors, cf. Fig. 1(a), are suppressed significantly. However, despite this, there is still a relatively high probability of randomly correlated hits early into the beam-off periods. This is shown in Table IV, in which the expected number of hits in all Ge crystals for prompt and delayed coincidences for different time intervals are compiled. The results demonstrate the significance of using a beam shut-off routine. Furthermore, due to many expected delayed coincidences as well as prompt coincidences during beam-on periods and within 5 ms after the beam pulse, these were excluded from the analysis. In conclusion, as few as three germanium hits were declared promptly coincident with ^{289}Fl full-energy α-decay events (chains 16 and 26 in Table I in the Supplemental Material of Ref. [2]). Based on the total of 47 α-decay events detected within the Fl-decay chains, about one is expected to stem from random correlations.

TABLE IV: Expected number of hits in all Ge crystals for different time intervals with respect to the start of the beam pulse. Prompt and delayed hits are those within $[-100, 300]$ ns and $[1,7]$ μs of the particle-triggered event, respectively.

Beam status	Interval (ms)	Delayed	Prompt
ON	[0,5]	20	1
OFF	[5,10]	10	0.6
	[10,15]	2	0.1
	[15,20]	0.8	0.04
	>100	0.3	0.02

[1] A. Såmark-Roth, D.M. Cox, D. Rudolph, L.G. Sarmiento, B.G. Carlsson, J.L. Egido, *et al.* Phys. Rev. Lett. **126**, 032503 (2021).
[2] D.M. Cox, A. Såmark-Roth, D. Rudolph, L.G. Sarmiento, R.M. Clark, J.L. Egido, *et al.*, submitted to Phys. Rev. C (L).
[3] U. Forsberg, D. Rudolph, L.-L. Andersson, A. Di Nitto, Ch.E. Düllmann, C. Fahlander *et al.*, Nucl. Phys. A **953**, 117 (2016).
[4] Ulrika Forsberg, Element 115, PhD thesis, Lund University, ISBN 978-91-7623-813-4 (pdf) (2016).
[5] L.-L. Andersson, D. Rudolph, P. Golubev, R.-D. Herzberg, R. Hoischen, E. Merchán, *et al.*, Nucl. Instr. Meth. **A 622**, 164 (2010).
[6] U. Forsberg, D. Rudolph, P. Golubev, L.G. Sarmiento, A. Yakushev, L.-L. Andersson *et al.*, Eur. Phys. J. Web of Conferences **66**, 02036 (2014).
[7] L.G. Sarmiento, L.-L. Andersson, and D. Rudolph, Nucl. Instr. Meth. **A 667**, 26 (2012).
[8] L.G. Sarmiento, EPJ Web of Conf. **131**, 05004 (2016).
[9] Anton Såmark-Roth, Spectroscopy along Decay Chains of Element 114, Flerovium, Lund University, ISBN 978-91-7895-836-8 (pdf) (2021).
[10] NNDC Evaluated Nuclear Structure Data File (ENSDF) Search and Retrieval. http://www.nndc.bnl.gov/ensdf/ (2016).
[11] G. Pausch, W. Bohne, and D. Hilscher, Nucl. Instr. Meth. **A 337**, 573 (1994).
[12] D.M. Cox, A. Såmark-Roth, D. Rudolph, L.G. Sarmiento, C. Fahlander, U. Forsberg, *et al.*, J. Phys. Conf. Ser. **1643**, 012125 (2020).
[13] Ch.E. Düllmann, M. Schädel, A. Yakushev, A. Türler, K. Eberhardt, J.V. Kratz *et al.*, Phys. Rev. Lett. **104**, 252701 (2010).
[14] J.M. Gates, Ch.E. Düllmann, M. Schädel, A. Yakushev, A. Türler, K. Eberhardt, *et al.*, Phys. Rev. C **83**, 054618 (2011).
[15] D. Rudolph, U. Forsberg, P. Golubev, L.G. Sarmiento, A. Yakushev, L.-L. Andersson *et al.*, Acta Phys. Pol. **B 45**, 263 (2014).
[16] Christian Lorenz, Quantum-state Selective Nuclear Decay Spectroscopy, PhD thesis, Lund University, ISBN 978-91-7753-943-8 (pdf).